Acoustical Efficiency of a Sonic Crystal Assisted Noise Barrier

F. Koussa[1]), J. Defrance[1]), P. Jean[1]), P. Blanc-Benon[2])

[1]) Centre Scientifique et Technique du Bâtiment, 24 rue Joseph Fourier, 38400 Saint Martin d'Hères, France.
faouzi.koussa@cstb.fr

[2]) Laboratoire de Mécanique des Fluides et d'Acoustique, UMR CNRS 5509, Ecole Centrale de Lyon,
Université de Lyon, 36 avenue Guy de Collongue, 69134 Ecully, France

Summary

This research work aims at evaluating the acoustic performance of a noise reducing device which combines sonic crystals with a conventional noise barrier. Numerical simulations, using a 2D Boundary Element Method (BEM), are carried out to evaluate their acoustic properties in terms of insertion and reflection losses due to the addition of the sonic crystal elements. The studied so-called sonic crystal assisted noise barrier is 3 m high and 1 m wide and is composed of two periodic bands of scatterers combined with a rigid straight barrier. Resonant cavities are used to produce extra insertion loss at some frequencies of resonance below the band gaps. Improved attenuation properties are found when resonant scatterers (cavities) and absorbent materials are combined. Our results show a significant extra insertion loss due to the addition of the sonic crystal elements for middle and high frequencies of typical road traffic noise. On the other hand, the extra reflection loss is limited.

PACS no. 43.50.Gf

1. Introduction

Sonic crystals (SC) are inhomogeneous materials made of regular arrays of scatterers embedded in a fluid medium. An interesting property of these materials is the occurrence of ranges of frequencies where no propagating modes are supported by the periodic structure. These ranges are known as band gaps (BG). The physical mechanism that explains this phenomenon is the destructive Bragg interference. The central frequency of the band gap f_{BG} is determined by the lattice constant α which presents the distance between adjacent scatterers for a square lattice,

$$f_{BG} = \frac{c}{2\alpha}, \tag{1}$$

where c is the speed of sound in air.

Three parameters play an important role in the band gap creation. The first one is the density ratio $M = \rho/\rho_0$ where ρ is the density of the material which constitutes the scatterers and ρ_0 is the density of air. The second parameter is the filling factor ff which expresses the ratio between the volume occuped by the scatterers V_s and the total volume V.

$$ff = \frac{V_s}{V} = \frac{\pi d^2}{4\alpha^2} \tag{2}$$

where d is the diameter of the scatterers.

The third parameter is the topology used for the design of the sonic crystal. A growing number of studies has been presented in the last two decades analyzing the propagation of acoustic waves inside sonic crystals. Several predictions models for such studies have been used such as the multiple scattering theory (MST) [1], the plane wave expansion (PWE) [2] and the modal scattering method (MSM) [3]. Sánchez *et al.* [4] studied the effectiveness of sonic crystals and showed that a two-dimensional arrangement of rigid hollow cylinders in air, with a small number of elements, can produce significant values of acoustic attenuation. The cylinders constituting a sonic crystal can be either hollow or solid. Vasseur *et al.* [5] showed theoretically and experimentally that the sonic crystal attenuation is the same for hollow or solid cylinders. This occurs for acoustic wavelengths that are larger than the size of each cylinder. Rigid scatterers like wood or aluminum have been used to study the physical behavior of sonic crystals when the reflection of acoustic waves becomes the mechanism of the band gap creation [6]. In addition, sonic crystals with mixed materials have been used to study the double effect of reflection and absorption on the frequency response of the sonic crystal [7]. Indeed, the use of soft cylinders is an alternative to solve the problem of the angular dependence of the acoustic attenuation. Resonant cylinders allow the sound to penetrate inside the elements of the periodic structure and as a consequence new acoustical properties can appear [8, 9, 10]. With this kind of scatterers a new attenuation band is obtained in the low frequency range which allows to reduce
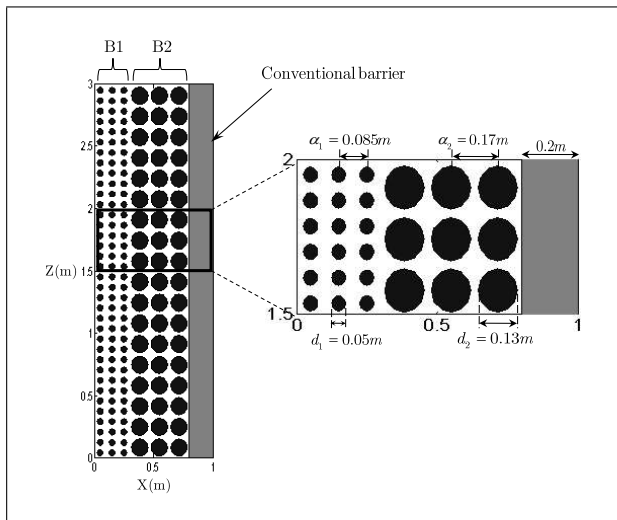
Figure 1. Scatterers arrangement in a sonic crystal in front of a conventional straight barrier.

the width of the sonic crystal. Romero-García *et al.* [11] studied theoretically and experimentally the acoustic performance of sonic crystals with added acoustical properties of resonance and absorption. They showed, for a periodic structure of perforated cylinders, that the periodicity of the perforations in the axis perpendicular to the plane of the crystal introduces a frequency band attenuation below the band gap. This band attenuation depends on the size of the interior cavity, on the radius of the perforation and on the distance between perforations. When the cylinders are filled with absorbent material, the authors showed that the sonic crystal have angular independence while maintaining the band attenuation due to the perforations.

The previous research works on sonic crystals considered their acoustical performance in the absence of a ground surface. In the presence of a ground surface, Krynkin *et al.* [12] studied the acoustical efficiency of regular arrays of cylinders with their axes parallel to the ground plane. They used a semi-analytical model based on multiple scattering theory and numerical simulations based on a boundary element formulation for rigid and impedance ground, respectively. The results of both methods were compared with experimental data. The authors showed that the performance of an array of cylinders above a rigid ground is similar to that of a doubled array composed of the original array plus an array corresponding to its mirror image in a rigid plane. The authors showed also that the first band gap was much reduced when it coincides with the destructive interference minimum due to the ground effect for some source-array-receiver configurations. The band gap was maintained for an impedance ground when ground effect minima were shifted to lower frequencies. These results are in agreement with those obtained by Romero-García *et al.* [13] showing the effect of a finite impedance surface on the acoustical performance of a sonic crystal using a semi-analytical model based on the multiple scattering theory and on the method of images.

Sonic crystals appear to be relatively efficient at some frequencies bands but are far less efficient than a conventional straight barrier. This is the reason why it is of interest to study their acoustical efficiency when they are combined with a straight noise barrier. We suppose that there is a sufficient space to insert a sonic crystal in front of a straight barrier. In this paper we evaluate with the BEM the extra insertion and reflection losses due to the addition of a sonic crystal system. The reflection loss is studied because of the higher levels experienced on the road due to regular barriers. The paper is divided in two parts: section 2 presents the sonic crystal assisted noise barrier design. In section 3, the numerical approach with the BEM is briefly described and convergence properties are discussed. Numerical results of insertion loss for realistic multi-lane traffic noise situations are presented for 2D and 3D noise sources. Reflection loss results are then presented using an inverse Fourier transform of the frequency BEM results.

2. Sonic crystal assisted noise barrier design

The geometry of the studied sonic crystal assisted noise barrier is given in Figure 1. It consists of two periodic bands of scatterers (BS1 and BS2) combined with a 3 m high rigid straight noise barrier. The first periodic band of scatterers BS1 extend from $x = 0$ m to $x = 0.30$ m with lattice constant $\alpha_1 = 0.085$ m. The scatterers used have a diameter $d_1 = 0.05$ m. The second periodic band BS2 extend from $x = 0.30$ m to $x = 0.80$ m with lattice constant $\alpha_2 = 0.17$ m. The diameter of the scatterers is $d_2 = 0.13$ m. The width of the straight noise barrier is 0.2 m. The first band of the sonic crystal is constituted by a periodic distribution of small scatterers. It increases the reflection loss effect when the wavelength is larger than the size of the scatterers. Using equation (1), the band gap of the first scatterers band will be created around 2000 Hz. The cylinders of the second band are larger than those of the first band. They are used to attenuate the frequency band around 1000 Hz where traffic noise has its main energy contribution.

In the following paragraphs, we present the efficiency results for different types of scatterers. Scatterers can be either rigid cylinders or resonant cavities. The cavities are either rigid or covered with an absorbent material in the interior. Results of reflection and insertion losses of the sonic crystal assisted barrier are reported when the axes of the scatterers are parallel to a reflecting ground.

3. Numerical approach for the assessment of sonic crystal assisted barriers efficiency

3.1. Boundary element method

In this research we use the BEM which allows to study complex shapes of scatterers combined with traditional

noise barriers for different impedance conditions. The BEM is a technique developed in the early sixties and is based on the integral equation theory [14, 15]. This method appears more appropriate in an infinite space than the finite element method because only the surface of the domain boundary must be discretized. Its main advantage is that it allows any kind of shape and impedance condition values on the surfaces to be accounted in a homogeneous atmosphere. The numerical code, MICADO [16], which we propose to use in this work is based on the direct integral equation formulation which can be expressed as

$$p(M) = t(M) + \int_S p(Q) \left(\rho\omega^2 Y(Q) G(M, Q) \right. $$
$$\left. - \frac{\partial G(M, Q)}{\partial n_Q} \right) \mathrm{d}S(Q). \quad (3)$$

In equation (3) the acoustic pressure p at any point M, for a source at any point Q, can be represented as the sum of a source term t and a radiated term. The radiated term is represented by an integral over the boundary S and is expressed in terms of the unknown pressure p, the Green function G and the admittance Y (ratio of velocity to pressure). The Green function describes the propagation of sound in the presence of an infinite ground and in the absence of diffracting objects. In this case, it is the sum of a direct term G_d, a reflected term G_r and a corrective term G_c which includes ground effects when the ground is not rigid [16]. It is given by

$$G(M, Q) = G_d(M, Q) + G_r(M, Q) + G_c(M, Q)$$
$$= -\frac{\mathrm{i}}{4} H_0(kr) - \frac{\mathrm{i}}{4} H_0(kr^-) + P_\alpha(M, Q), \quad (4)$$

where r is the (M, Q) distance, r^- is the distance between M and the image of Q with respect to the ground surface, H_0 is the Hankel function of the first kind and order zero and P_α is the correction factor for ground admittance.

The software MICADO uses a more complex approach based on a variational formalism where equation (3) is further developed and integrated a second time over S thus leading to a functional. The minimum of this functional also leads to a square symmetric matrix system. This approach provides a solution numerically more stable and the order of the singularities is reduced. Boundaries are meshed at each frequency automatically according to a criteria of minimum number of elements per wavelength and per segment, which greatly reduces computation times. The Hankel functions which appear in the elementary Green's terms are tabulated and interpolated when needed, which reduces the computation time required to compute the matrix by a factor of more than 20. The elementary integrations are done using Gauss integrations. In MICADO, the number of Gauss points NG may vary depending on the distance between points. These aspects make MICADO a specially optimized software in calculation time.

For sonic crystal elements, the objects to be meshed are the scatterers. They are discritized by means of straight elements. Previous calculations were carried out to ensure
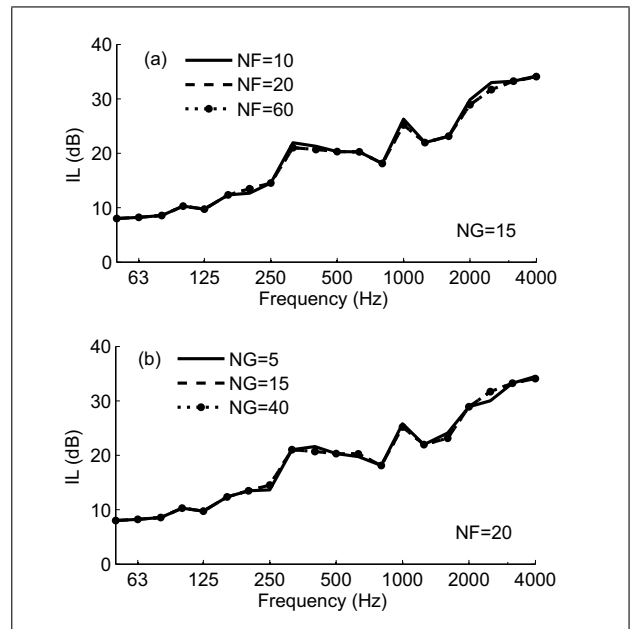

Figure 2. Efficiency of sonic crystal assisted noise barrier: effect of the frequency resolution NF (a) and the number of Gauss points NG (b) for convergence test.

convergence of calculations. Each scatterer is automatically split into a number of elements according to a double criteria (crit1,crit2); crit1 is the number of elements per acoustic wavelength λ and crit2 is the minimum number of elements per segment. In our case, the set (crit1,crit2) leading to convergence was found to be (3,12). The calculation time depends principally on the number of frequencies per third octave band NF and on the number of Gauss points NG for the computation of elementary matrices. Figure 2 shows the insertion loss (defined by equation (5) in section 3.2) results for different values of NF and NG. It shows that 20 frequencies per third octave band and 15 Gauss points are sufficient to ensure convergence of numerical calculations.

3.2. Insertion loss

3.2.1. Numerical simulations

In this section, the acoustic performance of sonic crystal assisted noise barriers along two-lane road is studied as shown in Figure 3. The width of each traffic lane is 4 m, both the street surface and pavement are modeled as rigid. Four sources are considered: two located at a height of 0.01 m (S2 and S4, representing light vehicle rolling noise emission) and two located 0.3 m above the road (S1 and S3, representing light vehicle engine noise emission). The noise sources are located in the middle of the road lanes. To calculate the global insertion loss in dB(A), the A-weighted road traffic noise spectra (for rolling and engine noises) calculated with weights according to the European Harmonoise model [17] are used.

The geometry of the problem is bi-dimensional: the source is an infinite linear coherent source and all the obstacles remain unchanged and infinite along a direction
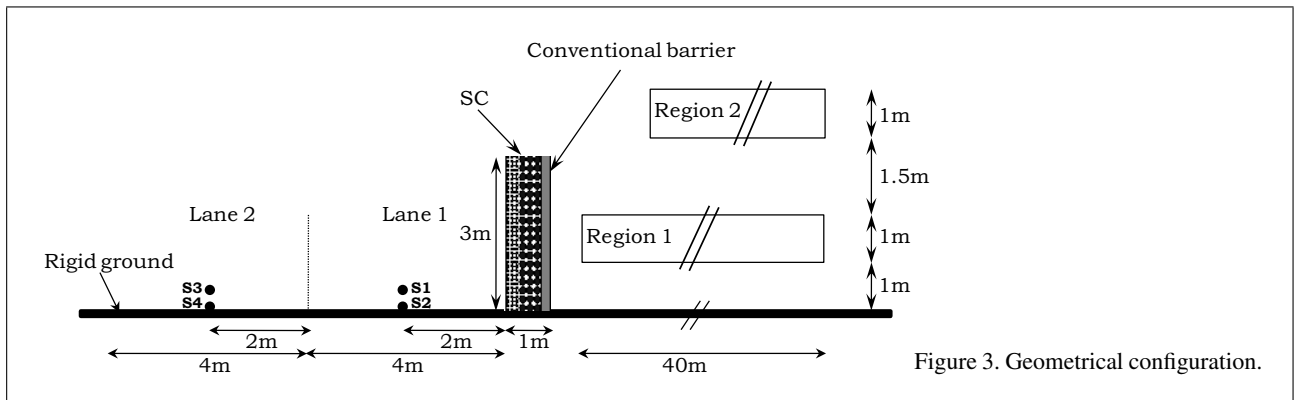
Figure 3. Geometrical configuration.

perpendicular to the vertical section plane. A homogeneous and windless atmosphere is assumed since the area of reception is close to the barrier. The reference case for all tests is the conventional rigid barrier (RB) without the sonic crystal. In this work, we investigate various sonic crystal assisted barriers with different properties. The scatterers of the two periodic bands are rigid cylinders, resonant cavities and absorbent cavities for sonic crystal assisted barriers SCAB1, SCAB2 and SCAB3, respectively (see Figure 4). SCAB2 and SCAB3 are proposed to add new acoustic effects different from those generated by the periodicity phenomenon. The absorbent material used to cover the interior of cavities in SCAB3 is a glass wool. It is characterized by a flow resistivity σ of $30\,\mathrm{kPa\,s/m^2}$ and is described using the one-parameter Delany and Bazley model [18]. For SCAB2 and SCAB3, the slot width (e_1) of the cavities of the first periodic band BS1 and that (e_2) of the cavities of the second periodic band BS2, has been selected to maximize the effect of resonance and absorption into the cavities (see Figure 5). It is found that the higher the slot width, the higher the insertion loss over the entire range of frequencies. This behavior could be assimilated to the Helmholtz resonators, where the resonant frequencies are proportional to the slot width and the size of the resonator cavity.

Two regions of receivers are defined behind the sonic crystal assisted barriers. Region 1 begins 1 m behind the barrier and extends 40 m at a height between 1 m and 2 m. It is representative of pedestrians and cyclists. Region 2 begins 10 m behind the barrier and extends 30 m at a height between 3.5 m and 4.5 m. It is representative of the first floor of a building. The two regions of receivers are defined with a precision of four receivers per meter in both x and y directions. The results are expressed as the average insertion loss per third octave band in the two regions of receivers.

3.2.2. Numerical results

Two types of results are presented here. First, the efficiency of sonic crystal assisted barriers is given as a function of frequency. Second, the results of the global effectiveness in dB(A), using a road traffic noise spectrum, are detailed.
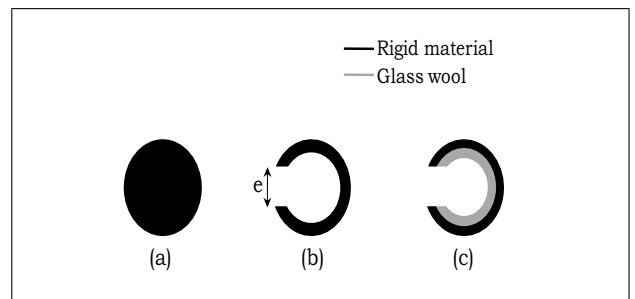

Figure 4. Scatterers used in the design of sonic crystal assisted barriers SCAB1 (a), SCAB2 (b) and SCAB3 (c).
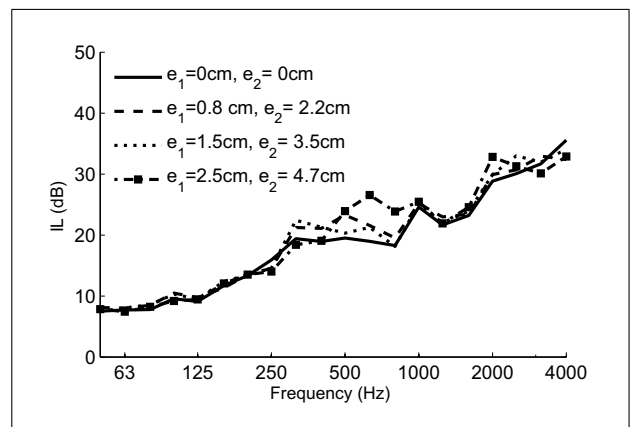

Figure 5. Effect of slots widths e_1 and e_2 of the cavities of BS1 and BS2 on the acoustic performance of sonic crystal assisted barrier SCAB2.

Insertion loss spectra

In this section we present numerical results of sonic crystal assisted barrier's insertion loss in real traffic noise situations. This insertion loss is the difference in received sound pressure level between the situations without and with the barrier, for the same source-receiver configuration. It indicates the true noise barrier benefit at the receiver.

Calculations are carried out taking 20 equally-spaced frequencies per third octave band. Previous calculations have shown that this is adequate to ensure convergence of calculations (see section 3.1). The frequency range of calculations has been chosen between 50 and 4000 Hz. This is a typical range used for road traffic noise studies.
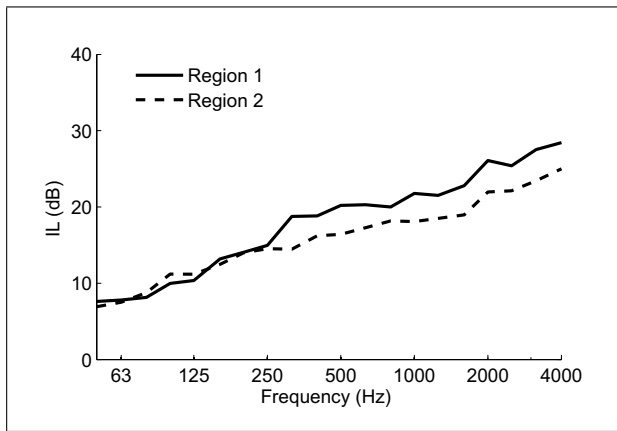
Figure 6. Insertion loss of the reference rigid barrier as a function of frequency: Region 1 (solid line) and Region 2 (dashed line).

The insertion loss for each third octave band is given by

$$IL_{\Delta f} = 10 \log_{10} \left(\left| \frac{P_{\text{ref}}(\Delta f)}{P_{\text{nb}}(\Delta f)} \right|^2 \right), \qquad (5)$$

where $|P_{\text{ref}}(\Delta f)|^2$ is the quadratic average over all receivers of the square acoustic pressure for the reference configuration without the noise barrier in the third octave band Δf and $|P_{\text{nb}}(\Delta f)|^2$ is the quadratic average over all receivers of the square acoustic pressure for the configuration with the noise barrier in the third octave band Δf. For the reference rigid barrier (RB), the efficiency results are presented using equation (5). The efficiency results for sonic crystal assisted barriers (SCAB) are presented as extra gains for the insertion loss relative to RB. The extra insertion loss $\Delta IL_{\text{SCAB},\Delta f}$ is given then by

$$\Delta IL_{\text{SCAB},\Delta f} = IL_{\text{SCAB},\Delta f} - IL_{RB,\Delta f}. \qquad (6)$$

The global source strength is obtained by summing the individual source energies (sources are considered incoherent with each other). The insertion loss spectra (IL) of the rigid barrier and the extra insertion loss spectra (ΔIL) of the different sonic crystal assisted barriers in the two regions of interest are given in Figure 6 and Figure 7, respectively. For all barriers, the shielding effect is higher in region 1 than in region 2. For receivers in region 1 which stand for pedestrians and cyclists, one can find only diffracted sound energy. In region 2, the direct sound contributions from sources increase and degrade the acoustic performance in comparison to region 1 especially when the vehicles are situated in lane 2.

From the analysis of the extra insertion loss produced by the sonic crystal assisted barriers, one can observe an increase in shielding with increasing frequency. For medium and high frequencies, the efficiency difference between the sonic crystal assisted barriers and the rigid barrier increases. The effect of rigid cylinders in SCAB1 is observed for some third octave bands. The extra insertion losses at 1000 Hz and 2000 Hz correspond to the band gaps created by the first and second periodic bands of cylinders. Indeed,
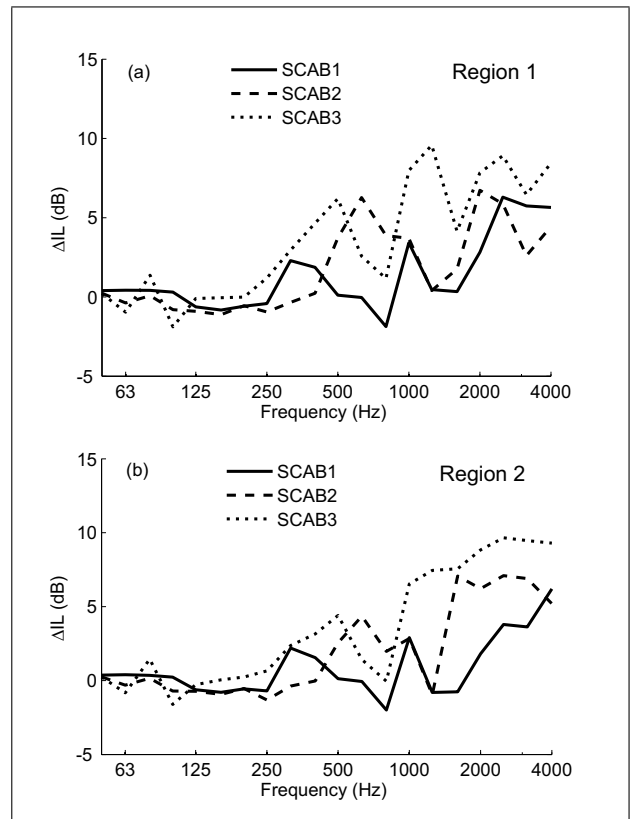

Figure 7. Extra insertion loss of sonic crystal assisted barriers as a function of frequency in Region 1 (a) and Region 2 (b): SCAB1 (solid line), SCAB2 (dashed line) and SCAB3 (dotted line).

the acoustic waves are attenuated before being diffracted by the top edge of the sonic crystal assisted barrier due to the periodicity phenomenon.

When the scatterers present some resonance properties, the performance of SCAB2 increases above the 250 Hz third octave band. The improvement of the global efficiency, in comparison to SCAB1, can reach 7 dB at 1600 Hz third octave band. To separate the effect of each band of scatterers (BS1 and BS2), we present in Figure 8 the results of insertion loss of each band by eliminating the other band of scatterers and the straight barrier. For every band, we compare the frequency response of both rigid cylinders and resonant cavities in presence of a reflective ground. When the cylinders are rigid, one can observe the presence of two band gaps centered around 2000 Hz and 1000 Hz for the first and the second band of cylinders, respectively. They are due to the multiple scattering by the cylinders (see equation 1). For resonant cavities, the insertion loss spectra present an increase of shielding for some third octave bands around 1600 Hz and 500 Hz for the first and the second band of scatterers, respectively. Indeed, the apparition of an additional attenuation should be result of a resonant behavior. This fact means that the effect of resonance and the Bragg's scattering appear at different frequency ranges. For SCAB3, we take advantage of the absorbent properties of the glass wool to improve the acoustic properties of the resonant cavities. In
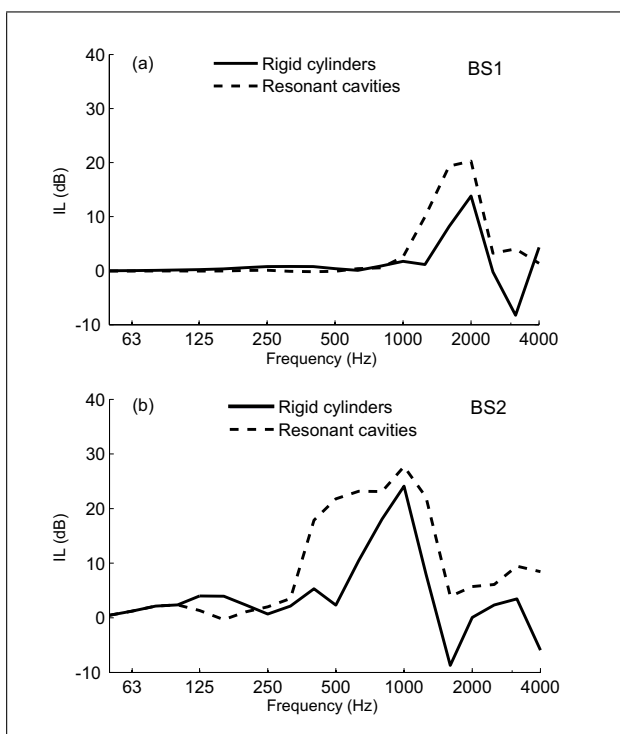
Figure 8. Insertion loss of the first periodic band BS1 (a) and the second periodic band BS2 (b): solid scatteres (solid line) and resonant cavities (dashed line).

Figure 7, one can observe an increase in extra insertion loss at medium and high frequencies when we combine resonant cavities with absorbent material. We can notice that the glass wool is efficient for all third octave bands above 250 Hz. The improvement due to the glass wool can reach 9.5 dB at 1250 Hz third octave band.

At low frequencies less than 250 Hz, the scatterers of the two first bands do not lead to an increase in shielding. Indeed, the wavelength at these frequencies is very large compared to the lattice constant and the propagation medium is considered homogeneous. However, low frequencies have a low weight in the calculation of the global efficiency (due to the road traffic noise spectrum). The global values of insertion loss in dB(A) are given in the following paragraph.

Global efficiency
The overall insertion loss in dB(A) is given by

$$IL_A = \tag{7}$$
$$10 \log_{10} \left(\frac{\sum\limits_{\Delta f} 10^{(L_{WR}+EA_{\text{ref},\Delta f})/10} + \sum\limits_{\Delta f} 10^{(L_{WP}+EA_{\text{ref},\Delta f})/10}}{\sum\limits_{\Delta f} 10^{(L_{WR}+EA_{\text{nb},\Delta f})/10} + \sum\limits_{\Delta f} 10^{(L_{WP}+EA_{\text{nb},\Delta f})/10}} \right),$$

where $EA_{\text{ref},\Delta f}$ is the excess attenuation calculated for the reference configuration without the noise barrier and for the third octave band Δf and $EA_{\text{nb},\Delta f}$ is the excess attenuation calculated in the configuration with the noise barrier and for the third octave band Δf. L_{WR} and L_{WP} are the road traffic noise sound power levels in third octave bands due to rolling and propulsion noise, respectively.

The global efficiency results, for the rigid barrier (RB), are presented using equation (7). Results for sonic crystal assisted barriers are extra gains for the global insertion loss relative to RB.

The global traffic noise insertion loss values of the rigid barrier and the global extra insertion loss values in dB(A) of the different sonic crystal assisted barriers are given in Table I. This is for different vehicles speeds (50, 70, 90 km/h) and for the two regions of reception. Three traffic noise situations are considered: one vehicle in lane 1, one vehicle in lane 2, two vehicles in lanes 1 and 2. The traffic configuration has an influence on the efficiency values and has the same effect for either receivers in region 1 or in region 2. Noise sources in lane 2 can contribute directly to the receivers of high altitude in region 2 and degrade the acoustic performance in comparison to region 1. In the two regions of reception and for all traffic noise situations, a larger insertion loss is observed with increasing vehicle speed when the rolling noise become more dominant.

The shielding due to SCAB1, SCAB2 and SCAB3 in the two regions of reception and for the three traffic noise situations is higher than that of the rigid barrier. As pointed out in Figure 7, the global values of extra insertion loss show that the acoustical efficiency of SCAB1 is not significant in comparison to the rigid barrier (RB). SCAB2 and SCAB3 offer more possibilities to improve the efficiency of a sonic crystal assisted barrier compared to the reference traditional barrier. For SCAB3, the global extra insertion loss can reach, for a vehicle speed of 90 km/h, 5.9, 4.8 and 5.8 dB(A) when considering one vehicle in lane 1, one vehicle in lane 2 or 2 vehicles in lanes 1 and 2, respectively. The absorption effect of SCAB3, compared to SCAB2, can reach 3 dB(A).

To sum up, Figure 7 and Table I show significant values of global insertion loss of sonic crystal assisted barriers compared to the reference thin conventional barrier located at $x = 0.8$ m. In this research work the insertion loss of sonic crystal assisted barriers is compared also to that of a rigid thick barrier positioned between $x = 0$ m and $x = 1$ m. The efficiency results for sonic crystal assisted barriers are presented as extra gains for the insertion loss relative to the thick barrier (ΔIL). The extra insertion loss spectra are given in Figure 9 for the two regions of receivers.

From the analysis of the extra insertion loss spectra, one can observe that sonic crystal assisted barriers are also more effective than the rigid thick barrier at medium and high frequencies. At low frequencies, a low degradation of the insertion loss is observed. The overall effectiveness of sonic crystal assisted barriers is higher than that of the thick barrier with a difference that can reach about 4 dB(A) for SCAB3.

In this paragraph the 2D spectra are computed for infinite coherent line source which does not describe a real noise traffic situation where the noise sources are rather incoherent. Therefore, in the following paragraph, we present the efficiency results of sonic crystal assisted

Table I. Global insertion loss of the rigid barrier RB and extra insertion loss of the sonic crystal assisted barriers SCAB1, SCAB2 and SCAB3 in the two regions of interest: Vehicle speed is 50, 70, 90 km/h. L1 denotes traffic lane 1, L2 denotes traffic lane 2.

| Traffic configuration		1 Vehicle in L1			1 Vehicle in L2			2 Vehicles in L1 and L2		
Vehicle speed (km/h)		**50**	**70**	**90**	**50**	**70**	**90**	**50**	**70**	**90**
RB (IL)	Region1	19.1	19.3	19.6	17.4	17.7	18.1	18.6	18.7	18.9
	Region2	16.9	17.1	17.5	15.3	15.5	15.9	16.3	16.5	16.8
SCAB1 (ΔIL)	Region1	2.1	2.3	2.5	1.4	1.7	1.9	1.8	2.1	2.3
	Region2	1.9	2.1	2.3	1.3	1.6	1.8	1.7	1.9	2.2
SCAB2 (ΔIL)	Region1	2.8	3.1	3.3	2.3	2.6	2.8	2.6	2.8	3.1
	Region2	3.3	3.7	3.9	2.8	3.1	3.4	3.1	3.4	3.7
SCAB3 (ΔIL)	Region1	4.6	4.9	5.1	4.1	4.3	4.5	4.3	4.6	4.9
	Region2	5.4	5.7	5.9	4.6	4.6	4.8	5.2	5.5	5.8
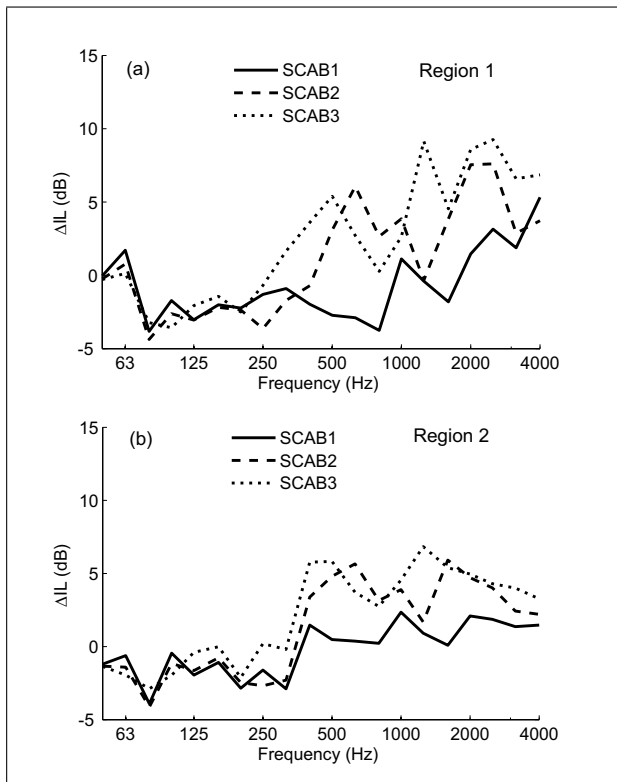
Figure 9. Extra insertion loss of sonic crystal assisted noise barriers as a function of frequency in Region 1 (a) and Region 2 (b): the refrence barrier is 1 m wide and 3 m high rigid thick barrier.

barriers for incoherent line sources. The effect of oblique incidence is taken into account using point sources.

3.2.3. Influence of the source type and the direction of propagation

Numerical simulations in the 2D domain imply that the geometry is two dimensional. In practice, the cross section of noise barriers does not vary in the third direction and the end diffraction effects are negligible. However, using a two dimensional excitation with an infinite coherent line of sources emitting in phase is not very realistic when the traffic noise sources are rather incoherent. A continuous sum of independent point sources is a good approximation

of an incoherent line source. It was demonstrated in the literature [19, 20] that it is possible to obtain the pressure field for point sources or incoherent line sources by simply post-processing 2-D results via a Fourier-type integration. Therefore, the aim of this section is to study the importance of source types when assessing the acoustic performance of sonic crystal assisted barriers in the case of road traffic noise. Point sources are used to estimate the oblique incidence effects whereas incoherent line sources are used to present the realistic case of traffic noise.

In a first step, the pressure field is obtained in the 2D domain. In a second step, a Fourier integral is used to calculate the 3D pressure field from the 2D pressure field [19],

$$P(x, y, z) = \frac{1}{2\pi} \int_{-\infty}^{\infty} p\left(x, y, z, Z(k)\frac{K}{k}\right) e^{-iaY} \, da, \qquad (8)$$

where P is the 3-D pressure at wave number K and position (x, y, z), p is the 2-D pressure at wave number k, and position (x, z), $k = \sqrt{K^2 - a^2}$, $Y = y - y_s$, where y_s is the y co-ordinate of the point source. $Z(k)$ represents the various impedances of the boundaries, including the infinite ground, at wave number k. The 2-D frequency spectrum necessary to compute the solution at K is limited to k which is less than or equal to K. When k becomes imaginary ($a > K$) the imaginary pressure solution decreases very rapidly with frequency and needs only be computed for the lower part of the 2-D spectrum.

In the case of an infinite continuous incoherent line source, the solution is obtained by integrating an infinite set of uncorrelated point sources. The squared ratio of total pressure to free field pressure is given by

$$A(x, y, z) = \frac{1}{2\pi} \int_{-\infty}^{\infty} \left| p\left(x, y, z, Z(k)\frac{K}{k}\right) \right|^2 \, da \qquad (9)$$

In the case of a finite line of uncorrelated point sources, contributions computed using equation (8) are simply summed in energy. When all of the boundaries are rigid, the computation of the 2-D spectrum needs only be calculated once. However, whenever impedances are introduced, either on the ground or on the obstacle, the modification of the Z spectra by the K/k factor implies the need
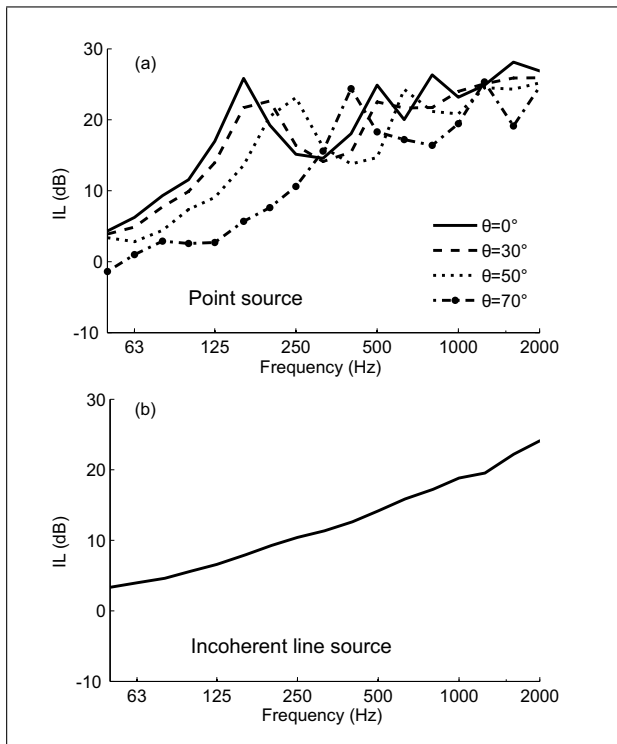
Figure 10. Effect of the source type on the insertion loss of the rigid barrier RB: point source (a) and finite incoherent line source (b).
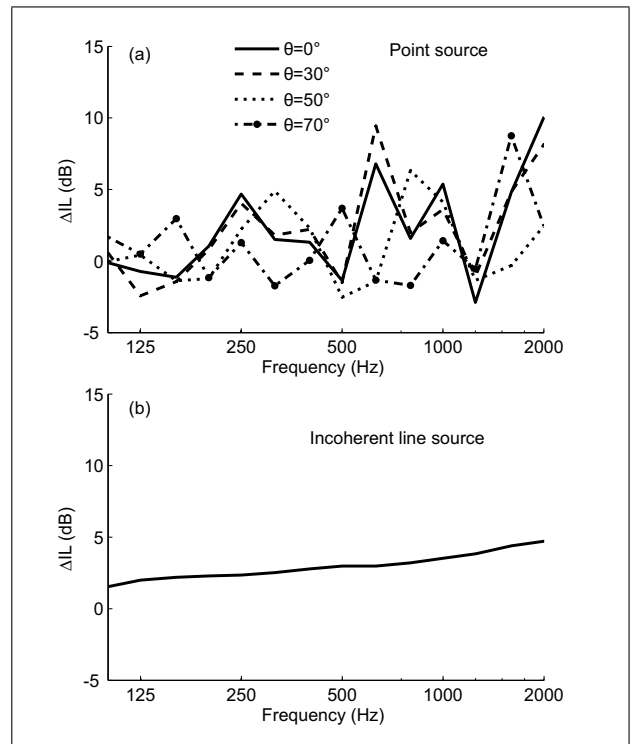

Figure 11. Effect of the source type on the extra insertion loss of the sonic crystal assisted barrier SCAB2: point source (a) and finite incoherent line source (b).

for a full computation of the 2-D solution, up to K, for every K. For this reason which implies an important increase in computation time, we present in this section results only for the thin rigid barrier RB located at x= 0.8 m and the sonic crystal assisted barrier SCAB2 and for a reduced frequency range between 50 and 2000 Hz.

For point sources and finite incoherent line sources, we represent in Figure 10 and Figure 11 the insertion loss of RB and the extra insertion loss of SCAB2, respectively. The results are presented for a receiver situated 10 m behind the barrier at a height of 1.5 m.

In the left graph in Figure 10 we compare the insertion loss of RB for four angles of propagation (four y positions between the point source and the receiver). It should be noted that the insertion loss with point source at normal incidence is very close to that with infinite coherent line source. The direction of propagation does not affect the efficiency for angles up to $\theta = 30°$. At $\theta = 50°$, the degradation, in comparison to the normal incidence, is not very important and does not exceed 3 dB(A). Beyond this angle the degradation becomes significant but the overall efficiency is still satisfactory.

In the right graph in Figure 10 we represent the insertion loss results in the case of a finite incoherent line source. A distribution of 120 point sources between −88° and +88° are sufficient to ensure convergence of results. A lower and smoother *IL* than that obtained with point sources is observed. It behaves like the average of all insertion loss spectra obtained for different angles (see Figure 10a). The global effectiveness is 19 dB(A) for 2D infinite coherent line and 15 dB(A) for 3D finite incoherent line.

In the left graph in Figure 11 we compare the extra insertion loss of SCAB2 for the four angles of propagation. An improvement of the acoustical efficiency, in comparison to the reference barrier (RB), is observed for some third octave bands for the different angles of incidence. Some peaks of extra insertion loss appear at different positions as a function of θ. Indeed, the position of the band gap depends on the lattice coefficient which varies depending on the direction of propagation.

In the right graph in Figure 11 we show the extra insertion loss spectrum of SCAB2 in the case of a finite incoherent line source. The effectiveness improvement increases with frequency with a maximum of 5 dB at 2000 Hz. At low frequencies, as demonstrated for coherent line sources, the efficiency difference between the sonic crystal assisted barrier and the reference rigid barrier is weak. The global extra insertion loss reach 3 dB(A) for 3D finite incoherent line.

Sonic crystal assisted barrier SCAB2 shows interesting values of attenuation whatever the source type or the direction of propagation. This show that sonic crystals can be used in combination with conventional noise barriers and offer high shielding. The following section shows the results of reflection loss which is an important parameter also in the assessment of noise barriers efficiency.

3.3. Reflection loss

3.3.1. Geometrical configuration

In this section the sound absorption of the sonic crystal assisted barrier will be studied by analyzing the tem-

poral field in front of the barrier in presence of a rigid ground. The temporary signals are obtained using an inverse Fourier transform of the pressure field calculated by the BEM sofware MICADO.

The configuration used to evaluate the reflection loss of the sonic crystal assisted barrier is given in Figure 12. The source is positioned 2 m from the barrier at the ground. On one hand, positioning the source at the ground presents a realistic case of road traffic noise, precisely the rolling noise. On the other hand, including the ground effect in the impulse response overcomes the problem of eliminating the reflections on the ground. Five point receivers are placed on an inclined line behind the sound source. This provides a path difference equal to or higher than 3 m between each point source and receiver. In this case, we can easily separate the incident and the reflected components of the impulse response. The temporal window can be long enough to contain almost all the reflected energy and to improve the low frequency limit. Indeed, the low frequency limit of sound reflection index is inversely proportional to the width of the analysis window.

In the following paragraph, the reflected signal by the sonic crystal assisted barrier is compared to that reflected by the rigid straight barrier without the sonic crystal.

3.3.2. Reflection index

The expression used to compute the reflection index RI_j as a function of frequency, in one-third octave bands, is given in the CEN/TS 1793-5:2003 standard [21] by

$$RI_j = \frac{1}{n_j} \sum_{k=1}^{n_j} \frac{\int_{\Delta n_j} \left| \text{FFT}\left[th_{\text{rSCAB},k}(t) w_{\text{rSCAB}}(t) \right] \right|^2 \mathrm{d}f}{\int_{\Delta n_j} \left| \text{FFT}\left[th_{\text{rRB},k}(t) w_{\text{rRB}}(t) \right] \right|^2 \mathrm{d}f}. \quad (10)$$

In this formula, j is the index of the one-third octave band and $n_j \leq 5$ is the number of receivers, $h_{\text{rSCAB},k}(t)$ and $h_{\text{rRB},k}(t)$ are the reflected signals at the $k - th$ angle by the sonic crystal assisted barrier and the rigid barrier, respectively. $w_{\text{rSCAB}}(t)$ and $w_{\text{rRB}}(t)$ are the sonic crystal assisted barrier reflected component time window and the rigid barrier component time window, respectively. The single-number rating of sound reflection DL_{RI}, in decibels, is given by [21]

$$DL_{RI} = -10 \log_{10} \left(\frac{\sum_{j=m}^{18} RI_j 10^{0.1 L_j}}{\sum_{j=m}^{18} 10^{0.1 L_j}} \right), \quad (11)$$

where L_j is the relative A-weighted sound pressure level (dB) of the normalized traffic noise spectrum, as defined in the EN 1793-3:1997 standard [22], in the $j - th$ one-third octave band. m is the index of the low third octave band limit. An example of the impulse response and the temporal window applied to the reflected component are given in the Figure 13 for sonic crystal assisted barrier SCAB2. The reflected signal contains a number of reflections by the scatterers, a peak corresponding to reflection by the rigid straight barrier (peak at 27 ms) and some attenuated peaks corresponding to a reflected energy after the penetration
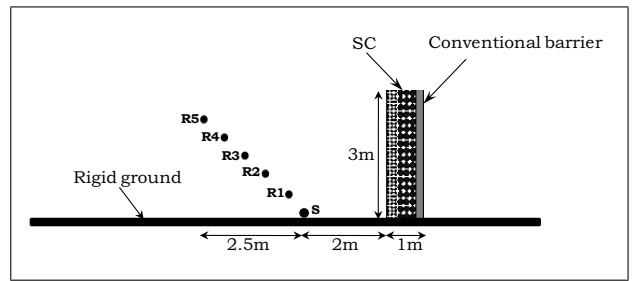

Figure 12. Geometrical configuration for the reflection loss assessment of the sonic crystal assisted barrier.
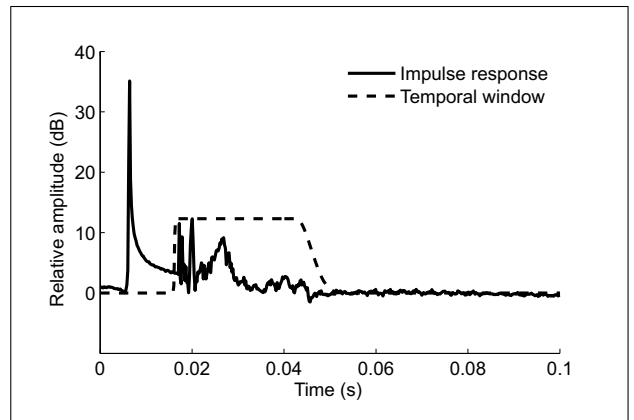

Figure 13. Impulse response (solid line) obtained by inverse Fourier transform and temporal windowing (dashed line) of the reflected field.

of the acoustic waves into the periodic array of scatterers. The temporal window must be long enough to contain almost all the reflected energy. In our case, the length of the temporal window is equal to 36 ms. This allows to reduce the low frequency limit to less than 50 Hz. The effect of diffraction by the top edge of the sonic crystal assisted barrier on the reflected field was studied by comparing the results for 3 m and 6 m high sonic crystal assisted barrier. The difference in terms of global pressure level does not exceed 0.1 dB(A). This allows to study subsequently the reflection properties of the sonic crystal assisted barrier with a low value of incertitude.

The results of the reflection index as a function of frequency for sonic crystal assisted barriers SCAB1, SCAB2 and SCAB3 are given in Figure 14. For SCAB1, the variation of the reflection index as a function frequency is almost constant. High values of reflection index (low reflection losses) for all third octave bands are observed. Indeed, the reflected signal contains a large number of reflections by the rigid cylinders. In addition, the straight rigid barrier returns a significant energy to the source side. The reflection response of SCAB2 is not very different from that of SCAB1. Low values of attenuation and insignificant improvement due to the resonance effect are observed. The dotted line in Figure 10 shows an increase in reflection loss at medium and high frequencies when resonant cavities and absorbent material are combined in SCAB3. The single number ratings of reflection loss DL_{RI} are 1 dB,
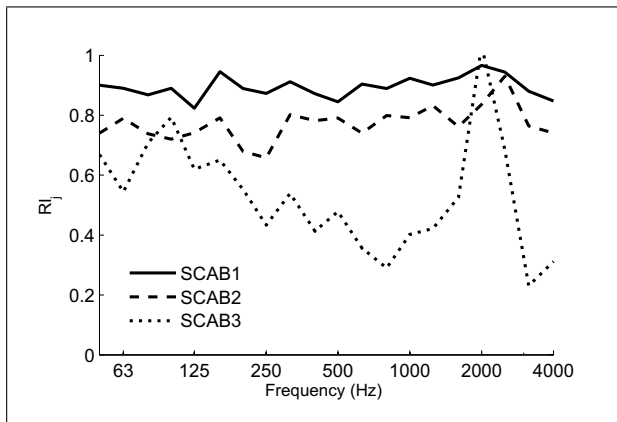
Figure 14. Reflection index as a function of frequency: SCAB1 (solid line), SCAB2 (dashed line) and SCAB3 (dotted line).

2 dB and 4 dB for sonic crystal assisted barriers SCAB1, SCAB2 and SCAB3, respectively. These values show, in this case, a weak effect in reflection for rigid cylinders and resonant cavities. For absorbent cavities, the reflective performance is average.

4. Conclusions

In this work, the evaluation of the extra insertion and reflection losses due to the addition of a sonic crystal elements to a straight noise barrier has been carried out numerically using a 2D BEM. Rigid cylinders, resonant cavities and absorbent cavities are used in the design of the sonic crystal. The sonic crystal assisted barrier insertion and reflection losses are studied and compared to those of the conventional barrier without the sonic crystal. 2D Insertion loss results showed high shielding of sonic crystal assisted barriers over the entire frequency range of road traffic noise when the sources are infinite and coherent. The improvement of the attenuation by diffraction, in comparison to the traditional barrier, can reach 6 dB(A) when sonic crystal assisted barrier present additional acoustic properties of resonance and absorption. Fourier-like transformation allows point sources or incoherent line sources to be considered simply by integrating the 2D results. Point sources are used to estimate the oblique incidence effects whereas incoherent line sources are used to present the realistic case of traffic noise. Sonic crystal assisted barriers present a non angular dependent insertion loss and high values of extra attenuation have been found even for very large angles. When line sources are incoherent, a lower and smoother insertion loss than that obtained with coherent line sources is observed. However, sonic crystal assisted barriers show high values of attenuation whatever the source type or the direction of propagation.

The reflection loss of sonic crystal assisted barriers have also been studied in this paper including the ground effect. Sonic crystal assisted barriers with added acoustical properties of resonance and absorption can attenuate the reflected acoustical field toward the source side in a quite limited range.

Our results show that sonic crystals can be used to improve the acoustical efficiency of traditional noise barriers. There is a wide choice of existing materials to construct sonic crystals like natural materials such as wood or recycled materials. These results open new perspective to the designing of sonic crystal assisted barriers. Using optimization algorithms, we could improve the attenuation capability of these noise barriers by using new arrangements of scatterers, changing the size and the shape of the scatteres or by creating a number of vacancies inside the sonic crystal assisted barrier. It could be also of importance to study whether sonic crystals may act as windbreaks when combined with straight barriers. It is what Van Renterghem and Botteldooren [23] showed in the case of a noise barrier combined with a row of trees behind: the modification of wind profiles induces a better performance of the barrier. Because sonic crystals are diffusers like trees are, it could therefore be interesting to check if we observe the same positive effect in the case of sonic crystal assisted noise barriers.

References

[1] V. Twersky: Multiple scattering of radiation by an arbitrary configuration of parallel cylinders. J. Acoust. Soc. Am. **24** (1952) 42–46.

[2] M. Kushwaha, P. Halevi, L. Dobrzynski, B. Djafari-Rouhani: Acoustic band structure of periodic elastic composites. Phys. Rev. Lett. **71** (1993) 2022–2025.

[3] N. Barrière: Étude théorique et expérimentale de la propagation du bruit de trafic en forêt. Ph.D. Thesis. Ecole Centrale de Lyon, France, 1999.

[4] J. V. Sánchez-Pérez, C. Rubio, R. Martínez-Sala, R. Sánchez-Grandia, V. Gómez: Acoustic barriers based on periodic arrays of scatterers. Appl. Phys. Lett. **81** (2002) 5240–5242.

[5] J. O. Vasseur, P. A. Deymier, A. Khelif, P. Lambin, B. Djafari-Rouhani, A. Akjouj, L. Dobrzynski, N. Fettouhi, J. Zemmouri: Phononic crystal with low filling fraction and absolute acoustic band gap in the audible frequency range: A theoretical and experimental study. Phys. Rev. E. **65** (2002) 056608.

[6] J. V. Sánchez-Pérez, D. Caballero, C. Rubio, R. Martínez-Sala, J. Sánchez-Dehesa, F. Meseguer, J. Llinares, F. Gálves: Sound attenuation by a two-dimensional arrays of rigid cylinders. Phys. Rev. Lett. **80** (1998) 5325–5328.

[7] O. Umnova, K. Attenborough, C. M. Linton: Effects of porous covering on sound attenuation by periodic arrays of cylinders. J. Acoust. Soc. Am. **119** (2006) 278–284.

[8] A. B. Movchan, S. Guenneau: Split-ring resonators and localized modes. Phys. Rev. B. **70** (2004) 125116.

[9] Z. Liu, X. Zhang, Y. Mao, Y. Zhu, Z. Yang, C. Chan, P. Sheng: Locally resonant sonic materials. Science **289** (2000) 1734–1736.

[10] A. Krynkin, O. Umnova, A. Y. B. Chong, S. Taherzadeh, K. Attenborough: Predictions and measurements of sound transmission through a periodic array of elastic shells in air. J. Acoust. Soc. Am. **128** (2010) 3496–3506.

[11] V. Romero-García, E. Fuster-Garcia, J. V. Sánchez-Pérez, L. M. García-Raffi: Sonic crystal acoustic barriers based on scatterers with added acoustical properties. Internoise, Lisbon, 2010.

[12] A. Krynkin, O. Umnova, J. V. Sánchez-Pérez, A. Y. B. Chong, S. Taherzadeh, K. Attenborough: Acoustic insertion loss due to two dimensional periodic arrays of circular cylinders parallel to a nearby surface. J. Acoust. Soc. Am. **130** (2011) 3736–3745.

[13] V. Romero-García, J. V. Sánchez-Pérez, L. M. García-Raffi: Analytical model to predict the effect of a finite impedance surface on the propagation properties of 2D sonic crystals. J. Phys. D: Appl. Phys. **44** (2011) 265501.

[14] R. D. Ciskowski, C. A. Brebbia: Boundary element methods in acoustics. Elsevier Applied Science, London, 1991.

[15] S. Kirkup: The boundary element methods in acoustics. Integrated Sound Software, 2007.

[16] P. Jean: A variational approach for the study of outdoor sound propagation and application to railway noise. J. Sound and Vib. **212** (1998) 275–294.

[17] H. Jonasson, U. Sandberg, G. Van Blokland, J. Ejsmont, G. Watts, M. Luminari: Source modelling of road vehicles. Deliverable 9 of the Harmonoise project, Technical report HAR11TR-041210-SP10, 2004.

[18] M. E. Delany, E. N. Bazley: Acoustical properties of fibrous absorbent materials. Appl. Acoust. **3** (1970) 105–116.

[19] D. Duhamel: Efficient calculation of the three-dimensional sound pressure field around a noise barrier. J. Sound and Vib. **197** (1996) 547–571.

[20] P. Jean, J. Defrance, Y. Gabillet: The importance of source type on the assessment of noise barriers. J. Sound and Vib. **226** (1999) 201–216.

[21] European Standard CEN/TS 1793-5: Road traffic noise reducing devices – Test method for determining the acoustic performance – Part 5: Intrinsic characteristics – In situ values of sound reflection and airborne sound insulation. 2003.

[22] European Standard EN 1793-3: Road traffic noise reducing devices – Test method for determining the acoustic performance – Part 3: Normalized traffic noise spectrum. 1997.

[23] T. Van Renterghem, D. Botteldooren: Effect of a row of trees behind noise barriers in wind. Acta Acustica united with Acustica **88** (2002) 869–878.